iScience

CellPress
OPEN ACCESS

Article

Neuronal XRN1 is required for maintenance of whole-body metabolic homeostasis

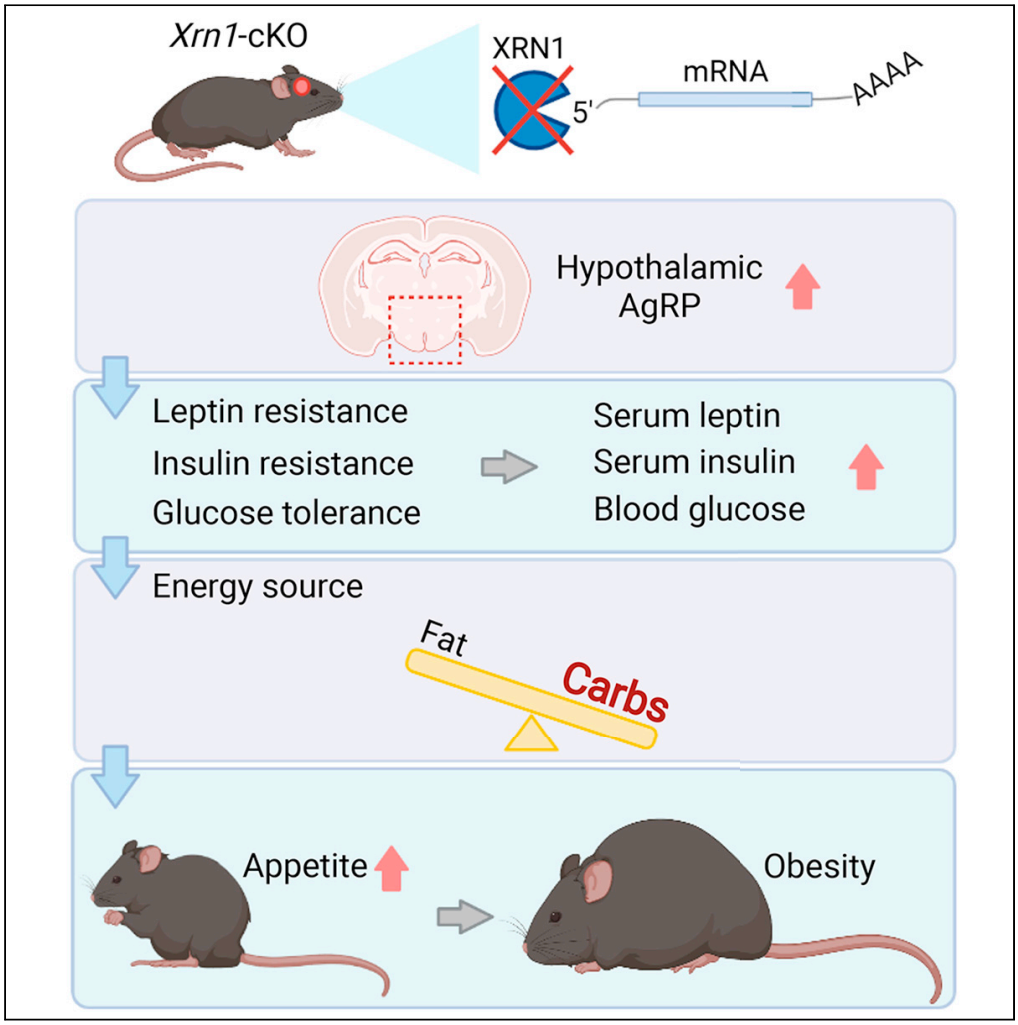

Shohei Takaoka, Akiko Yanagiya, Haytham Mohamed Aly Mohamed, ..., Akinori Takahashi, Patrick Stoney, Tadashi Yamamoto

akiko.yanagiya@oist.jp (A.Y.)
haytham.mohamed@oist.jp (H.M.A.M.)
tadashi.yamamoto@oist.jp (T.Y.)

Highlights

Forebrain specific *Xrn1*-cKO mice exhibit obesity with hyperphagia

Xrn1-cKO mice exhibit leptin resistance, insulin resistance, and impaired glucose tolerance

Xrn1-cKO mice cannot utilize fat as an energy source and mainly use carbohydrate

AgRP expression is upregulated in the *Xrn1*-cKO hypothalamus

Takaoka et al., iScience *24*, 103151
October 22, 2021
https://doi.org/10.1016/j.isci.2021.103151

iScience

CellPress
OPEN ACCESS

Article

Neuronal XRN1 is required for maintenance of whole-body metabolic homeostasis

Shohei Takaoka,[1] Akiko Yanagiya,[1,*] Haytham Mohamed Aly Mohamed,[1,4,*] Rei Higa,[1,2] Takaya Abe,[3] Ken-ichi Inoue,[3] Akinori Takahashi,[1] Patrick Stoney,[1] and Tadashi Yamamoto[1,5,*]

SUMMARY

Control of mRNA stability and degradation is essential for appropriate gene expression, and its dysregulation causes various disorders, including cancer, neurodegenerative diseases, diabetes, and obesity. The 5′–3′ exoribonuclease XRN1 executes the last step of RNA decay, but its physiological impact is not well understood. To address this, forebrain-specific *Xrn1* conditional knockout mice (*Xrn1*-cKO) were generated, as *Xrn1* null mice were embryonic lethal. *Xrn1*-cKO mice exhibited obesity with leptin resistance, hyperglycemia, hyperphagia, and decreased energy expenditure. Obesity resulted from dysregulated communication between the central nervous system and peripheral tissues. Moreover, expression of mRNAs encoding proteins that regulate appetite and energy expenditure was dysregulated in the hypothalamus of *Xrn1*-cKO mice. Therefore, we propose that XRN1 function in the hypothalamus is critical for maintenance of metabolic homeostasis.

INTRODUCTION

Obesity is an increasingly serious global health issue and it is associated with many metabolic disorders, such as type 2 diabetes and cardiovascular disease. Therefore, understanding the molecular pathology of obesity is critical. Obesity is caused by an imbalance between energy intake and energy expenditure. Whole-body energy metabolism is controlled by communication between the central nervous system and peripheral metabolic tissues, including adipose tissue, liver, pancreas, and skeletal muscle (Myers and Olson, 2012). The hypothalamus integrates inputs from various peripheral tissues and regulates feeding and energy expenditure (Timper and Brüning, 2017). Therefore, various studies have sought to identify hypothalamic nuclei and neuropeptides involved in eating and regulation of energy metabolism.

The importance of post-transcriptional regulation, including mRNA degradation, for proper gene expression is increasingly appreciated, because changes in mRNA decay affect transcript levels and subsequent protein abundance (Chen and Shyu, 2011; Garneau et al., 2007). Moreover, alterations of mRNA stability have been reported in cancer, neurodegenerative disease, diabetes, and obesity (Audic and Hartley, 2004; Linder et al., 2015; Mang et al., 2015). Eukaryotic mRNAs have two characteristic structures, a 7-methyl guanosine cap (m^7G cap) at the 5′ end and a poly(A) tail at the 3′ end, which provide effective protection against exoribonucleases and contribute to mRNA stability (Chen and Shyu, 2011; Garneau et al., 2007). In normal mRNA degradation, the first step is shortening of the 3′ poly(A) tail, a process called deadenylation, regulated by the CCR4-NOT complex and PAN2-PAN3 (Chen and Shyu, 2011; Garneau et al., 2007). After deadenylation, the m^7G cap structure is removed from the deadenylated mRNA by the DCP1-DCP2 decapping complex. Finally, deadenylated and decapped mRNAs are degraded by the major cytoplasmic 5′–3′ exoribonuclease XRN1 (Garneau et al., 2007).

These mRNA degradation factors serve multiple functions in gene expression and are responsible for various physiological processes. Not surprisingly, deletion of mRNA degradation machinery leads to various physiological defects in animal models. For example, mutations in CCR4-NOT subunits in mouse cause defects in energy metabolism, adipocyte and heart function, and maturation of the liver and pancreatic β-cells (Morita et al., 2011; Mostafa et al., 2020; Suzuki et al., 2019; Takahashi et al., 2015, 2019, 2020; Yamaguchi et al., 2018).

Compared to the well-investigated CCR4-NOT deadenylation complex, physiological studies of 5′–3′ exonucleases in vertebrates are few. In yeast, disruption of the 5′-to-3′ exoribonuclease, *Xrn1*, causes severe

[1]Cell Signal Unit, Okinawa Institute of Science and Technology Graduate University, 1919-1 Tancha, Onna, Okinawa 904-0495, Japan

[2]Department of Bioresources Engineering, National Institute of Technology, Okinawa College, 905 Henoko, Nago, Okinawa 905-2192, Japan

[3]Laboratory for Animal Resources and Genetic Engineering, RIKEN Center for Biosystems Dynamics Research, 2-2-3 Minatojima Minami-machi, Chuou-ku, Kobe 650-0047, Japan

[4]Present address: Division of Genetics, Department of Cancer Biology, The Institute of Medical Science, The University of Tokyo, 4-6-1, Shirokanedai, Minato-ku, Tokyo 108-8639, Japan

[5]Lead contact

*Correspondence: akiko.yanagiya@oist.jp (A.Y.), haytham.mohamed@oist.jp (H.M.A.M.), tadashi.yamamoto@oist.jp (T.Y.)

https://doi.org/10.1016/j.isci.2021.103151

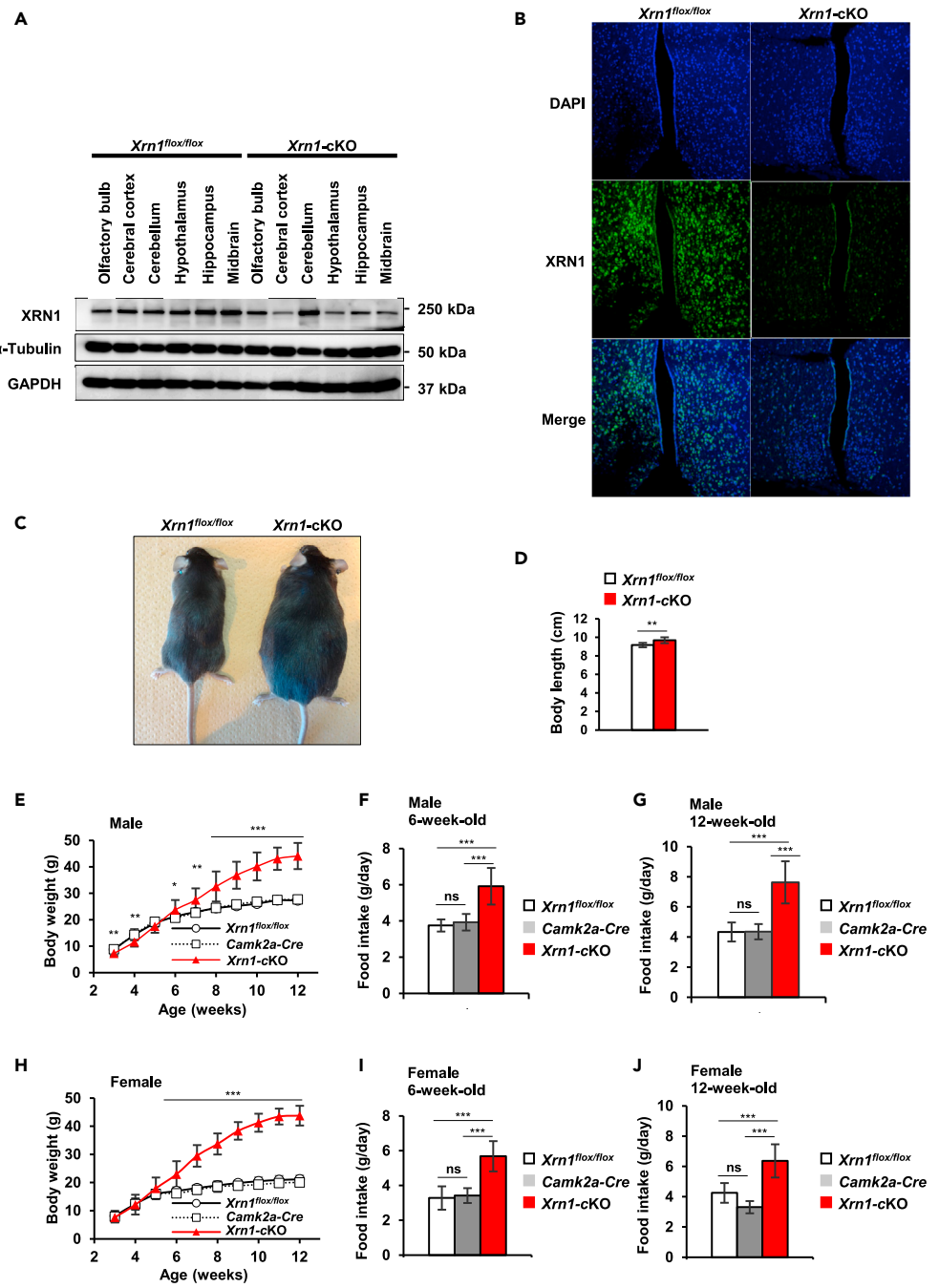

Figure 1. *Camk2a-Cre*-mediated deletion of *Xrn1* in brain causes obesity and hyperphagia

(A) XRN1, α-Tubulin, and GAPDH in brain lysates from 12-week-old *Xrn1*-cKO and control ($Xrn1^{flox/+}$) mice are shown by western blotting.

(B) XRN1 expression (green) in the hypothalamus of 5-week-old male $Xrn1^{flox/flox}$ and *Xrn1*-cKO mice is shown by immunofluorescence staining. Nuclei were shown by DAPI staining (blue).

(C) 12-week-old male $Xrn1^{flox/flox}$ and *Xrn1*-cKO littermates are shown.

(D) Body lengths (nose-to-anus) of male 12-week-old $Xrn1^{flox/flox}$ (white, n = 7) and *Xrn1*-cKO mice (red, n = 6).

(E–J) Growth curve of $Xrn1^{flox/flox}$ (white circle, n = 10), *Camk2a-Cre* (white square, n = 10) and *Xrn1*-cKO male (red triangle, n = 10) (E) and female (H) mice from 3 to 12 weeks old. Data represent means ± SD. One-way ANOVA between $Xrn1^{flox/flox}$

Figure 1. *Continued*
and *Xrn1*-cKO mice *p < 0.05; **p < 0.01; and ***p < 0.001. (F, G, I and J) Average daily food intake of male $Xrn1^{flox/flox}$ (white, n = 10), *Camk2a-Cre* (gray, n = 10) and *Xrn1*-cKO (red, n = 10) male (F and G) and female (I and J) mice at 6 weeks old (F and I) or 12 weeks old (G and J). Data represent mean ± SD. One-way ANOVA, Tukey post hoc test, *p < 0.05; **p < 0.01; and ***p < 0.001.

growth defects (Larimer and Stevens, 1990). siRNA-mediated knockdown of *Xrn1* in *C. elegans* causes embryonic lethality due to failure of ventral epithelial enclosure during embryogenesis (Newbury and Woollard, 2004). Interestingly, hypomorphic mutations in Pacman, the *Drosophila* homolog of *Xrn1*, also cause defects in dorsal/thorax closure and epithelial sheet sealing that participates in ventral epithelial enclosure in *C. elegans* (Grima et al., 2008; Jones et al., 2012). Pacman is required for both male and female fertility in *Drosophila*, as mutations cause defects in spermatogenesis and oogenesis (Lin et al., 2008; Zabolotskaya et al., 2008). These studies in invertebrates clearly indicate the importance of XRN1, but little is known about its physiological role in mammals.

In this study, we established a knockout mouse model to investigate the physiological function of XRN1. We provide evidence that a lack of XRN1 in neurons leads to obesity accompanied by leptin resistance, hyperglycemia, hyperinsulinemia, hyperleptinemia, hyperphagia, and decreased energy expenditure in mice. XRN1 depletion leads to aberrant expression of hypothalamic genes associated with regulation of appetite and energy homeostasis. Our study demonstrates that XRN1 in the brain is required for maintenance of whole-body energy homeostasis.

RESULTS

Forebrain-specific disruption of *Xrn1* causes severe obesity associated with hyperphagia

Little is known about the physiological functions of XRN1, due in part to a lack of knockout (KO) mice. To investigate the physiological functions of XRN1, floxed mice were generated ($Xrn1^{flox/flox}$ mice) with *loxP* sites flanking exons 2 to 6 of the *Xrn1* gene (Figure S1A). The resulting $Xrn1^{flox/+}$ mice were crossed with *CAG-Cre* mice to establish whole-body *Xrn1*-KO mice. Whole-body *Xrn1*-KO mice were embryonic lethal at around E10.5, whereas $Xrn1^{+/-}$ mice were viable and fertile without obvious defects (Figure S1B). Whole-body *Xrn1*-KO embryos exhibit poor growth with incomplete neural tube closure (Figure S1B). Defects in epithelial closure are also observed in *Drosophila* and *C. elegans* with XRN1 mutations (Grima et al., 2008; Newbury and Woollard, 2004), suggesting a conserved role in these processes between species.

XRN1 regulates synaptic activity by forming postsynaptic XRN1 bodies (SX-bodies), which contribute to suppression of protein synthesis in response to N-methyl-D-aspartate receptor (NMDAR) stimulation in cultured hippocampal neurons (Luchelli et al., 2015), suggesting that XRN1 contributes to neural function. To investigate the requirement of XRN1 in the brain, we generated conditional *Xrn1* knockout mice. $Xrn1^{flox/flox}$ mice were crossed with *Camk2a-Cre* mice, which express Cre in a large population of excitatory neurons in the forebrain (Casanova et al., 2001). XRN1 protein levels were reduced in the cerebral cortex, hippocampus and hypothalamus of forebrain-specific *Xrn1* conditional knockout (*Xrn1*-cKO) mice (Figure 1A). Immunofluorescence staining using XRN1 antibody revealed reduced XRN1 expression in the hypothalamus of *Xrn1*-cKO mice compared to $Xrn1^{flox/flox}$ mice (Figure 1B). Notably, 12-week-old *Xrn1*-cKO mice exhibited longer body lengths than those of control mice (Figures 1C and 1D). Around weaning at 3–4 weeks old, the body weight of male *Xrn1*-cKO mice was significantly lower than that of control mice, whereas the body weight of female *Xrn1*-cKO mice did not differ from that of control mice at this age. However, *Xrn1*-cKO mice rapidly gained weight after 5 weeks old, and the body weight of both male and female *Xrn1*-cKO mice increased significantly after 6 weeks old (Figures 1E and 1H). Next, we examined daily food intake in both young (6-week) and adult (12-week) mice. Mice were individually housed and daily food intake was measured. Food intake of *Xrn1*-cKO mice was significantly higher in both male and female mice that are older than 6 weeks (Figures 1F, 1G, 1I, and 1J). Therefore, depletion of XRN1 in forebrain neurons causes obesity associated with hyperphagia in both male and female mice.

Depletion of XRN1 in mouse brain leads to severe adiposity and fatty liver

To confirm that deletion of XRN1 in *Xrn1*-cKO mice was specific to the brain, we examined XRN1 protein expression in peripheral tissues associated with metabolic homeostasis. XRN1 protein expression was unchanged in thymus, inguinal white adipose tissue (iWAT), pancreas, and muscle (Figure 2A). In *Xrn1*-cKO mice, weights of iWAT, epididymal white adipose tissue (eWAT), brown adipose tissue (BAT), and liver

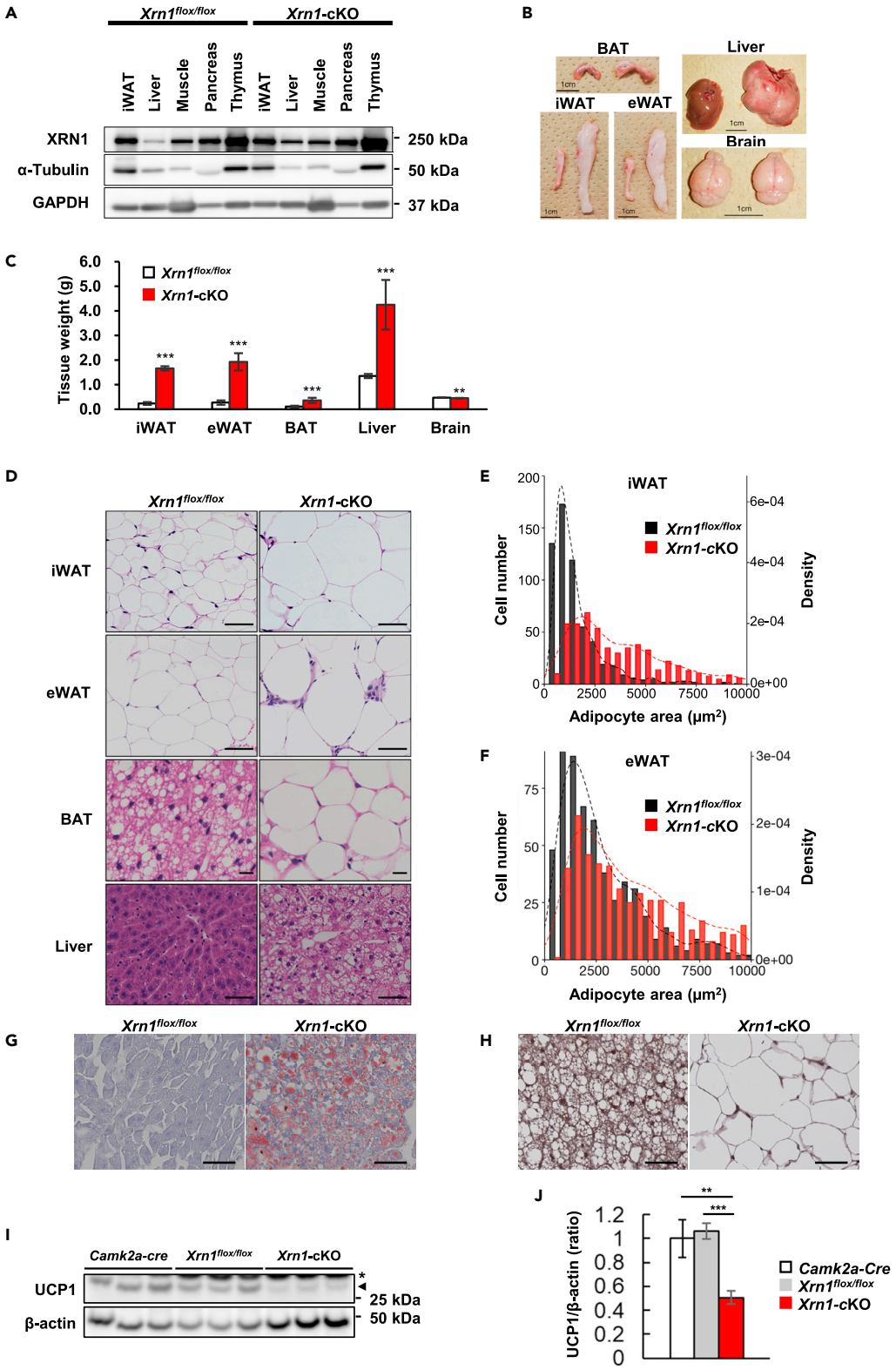

Figure 2. *Xrn1*-cKO mice exhibit aberrant adiposity and liver steatosis

(A) Immunoblotting for XRN1, α-Tubulin, and GAPDH in peripheral tissue lysates from *Xrn1*-cKO and control ($Xrn1^{flox/+}$) mice at 12 weeks old.

Figure 2. *Continued*

(B) White adipose tissues (eWAT and iWAT), BAT, liver and brain from male 12-week-old *Xrn1*$^{flox/flox}$ (left) and *Xrn1*-cKO (right) littermates.

(C) Tissue weights of *Xrn1*$^{flox/flox}$ (white, n = 5–8) and *Xrn1*-cKO (red, n = 3–7) mice at 12 weeks old. Data represent means ± SD. Unpaired Student's t test, **p < 0.01; ***p < 0.001.

(D) HE-stained paraffin sections of iWAT, eWAT, BAT and liver from 23-week *Xrn1*$^{flox/flox}$ (left) and *Xrn1*-cKO (right) mice. Black scale bars represent 50 μm.

(E and F) Histograms of adipocyte size in iWAT (E) and eWAT (F) of *Xrn1*$^{flox/flox}$ (black) and *Xrn1*-cKO (red) mice are shown.

(G) Lipid accumulation in the liver of *Xrn1*-cKO compared to that of *Xrn1*$^{flox/flox}$ mice by Oil Red O staining.

(H) Decreased UCP1 expression in BAT of *Xrn1*-cKO compared to that in *Xrn1*$^{flox/flox}$ mice by immunohistochemistry.

(I) Protein expression of UCP1 and β-actin in BAT of *Camk2a-Cre*, *Xrn1*$^{flox/flox}$ and *Xrn1*-cKO mice (n = 3) is shown by western blotting. An arrow and an asterisk indicate UCP1 and non-specific bands, respectively.

(J) Band intensities in Figure 2I were measured using NIH ImageJ. Average values from *Camk2a-Cre* mice were set as 1. Data represent means ± SEM. Unpaired Student's t test, *p < 0.05; **p < 0.01; and ***p < 0.001.

mass were increased, whereas brain mass was less than that of control littermates (Figures 2B and 2C). Hematoxylin and eosin (HE) staining revealed that adipocytes in iWAT and eWAT from 23-week-old *Xrn1*-cKO mice were drastically enlarged compared to those of *Xrn1*$^{flox/flox}$ mice. Aberrant lipids accumulated in adipocytes in BAT from 23-week-old *Xrn1*-cKO mice, demonstrating disruption of lipid metabolism (Figures 2D, 2E, and 2F). Oil red O staining revealed that lipids accumulated in livers of *Xrn1*-cKO mice compared to those of *Xrn1*$^{flox/flox}$ mice, suggesting aberrant lipid metabolism in liver (Figure 2G) and systematic dysregulation of metabolism in *Xrn1*-cKO mice. Finally, immunohistochemistry of brown adipose tissue (BAT) from *Xrn1*-cKO mice suggested that uncoupling protein 1 (UCP1) was reduced compared to that in *Xrn1*$^{flox/flox}$ mice (Figure 2H) and this reduction was confirmed by western blotting (Figures 2I and 2J). UCP1 regulates the thermogenic capacity of adipocytes and contributes to regulation of energy expenditure and its decrease implies impaired lipid metabolism in *Xrn1*-cKO mice.

Peripheral metabolism is altered before the onset of obesity in *Xrn1*-cKO mice

Because *Xrn1*-cKO mice exhibit hyperphagia, increased body weight, and fat accumulation, we hypothesized that communication between the central nervous system including the hypothalamus and peripheral metabolic tissues was impaired because of the lack of XRN1. To investigate the mediator of inter-organ communication, blood glucose, serum insulin, and serum leptin were monitored, since a prolonged increase of these metabolites is associated with development of obesity. To determine whether increased leptin, insulin, or glucose are a cause or consequence of obesity in *Xrn1*-cKO mice, these parameters were measured in 5-week-old mice before the onset of obesity. Serum leptin was already significantly increased in 5-week-old *Xrn1*-cKO mice compared to control mice, suggesting that alteration of peripheral metabolic signals had already developed before the onset of obesity (Figure 3A). Although serum insulin varied between individual *Xrn1*-cKO mice, there was a tendency toward increased insulin at 6 weeks old (p = 0.0501; Figure S2A).

Blood glucose (measured at 13 weeks old), serum insulin (14 weeks old), and serum leptin (15 weeks old) were significantly higher in adult *Xrn1*-cKO mice than in control mice (Figure S2B). Because blood glucose in 5-week and 6-week-old *Xrn1*-cKO mice was not significantly different from that of control mice, an increase of insulin and leptin occurs first, which may drive the subsequent hyperglycemia observed in adult *Xrn1*-cKO mice. Notably, *Xrn1*-cKO mice are hyperphagic despite elevated serum leptin, implying leptin resistance in the hypothalamus. Leptin sensitivity was assessed in *Xrn1*-cKO mice and their control (*Xrn1*$^{flox/flox}$) littermates at 5 weeks of age, when *Xrn1*-cKO mice do not exhibit obesity. Mice were treated daily with leptin via intraperitoneal (IP) injection, and body weight and food intake were measured each day. Before leptin treatment, food intake of 5-week-old *Xrn1*-cKO mice was increased compared to control littermates (Figure S3C). Body weight and food intake were suppressed by leptin in *Xrn1*$^{flox/flox}$ mice, but not in *Xrn1*-cKO littermates (Figures 3B and 3C), revealing that *Xrn1*-cKO mice developed leptin resistance before the onset of obesity.

To investigate the onset of hyperglycemia in *Xrn1*-cKO mice, fed and fasting blood glucose were monitored at 5, 7 and 9 weeks old. Both fed and fasting blood glucose were significantly increased in 9-week-old *Xrn1*-cKO mice compared to control mice (p < 0.05 and p < 0.001, respectively) (Figure 3D). Moreover, glucose tolerance was impaired in 5-week-old *Xrn1*-cKO mice compared to control mice (Figure 3E), indicating that glucose metabolism is dysregulated in *Xrn1*-cKO mice. Furthermore, 5-week-old *Xrn1*-cKO mice exhibited insulin resistance (Figure 3F), suggesting that insulin sensitivity is impaired in

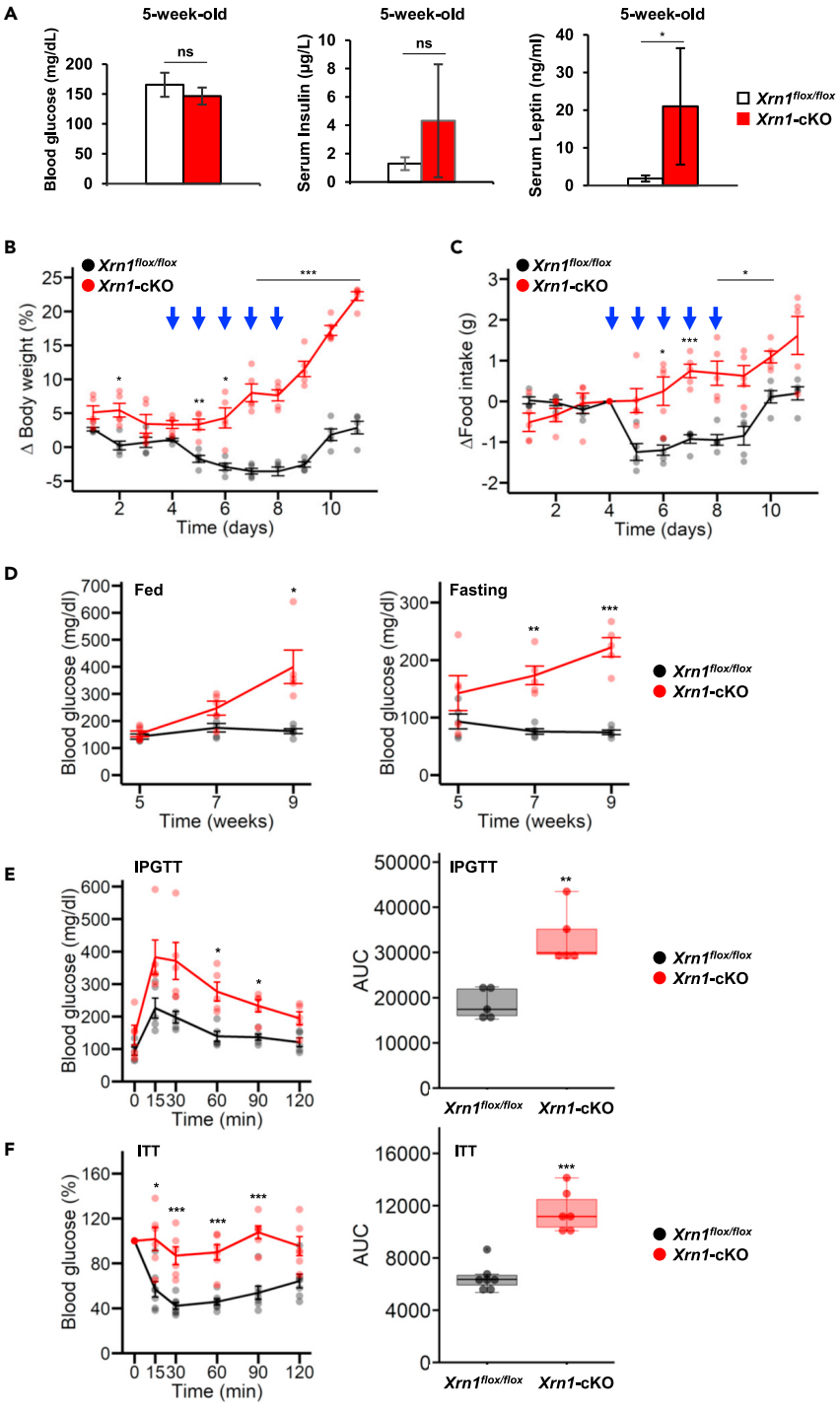

Figure 3. *Xrn1*-cKO mice exhibit metabolic disorders with hyperglycemia, hyperinsulinemia, and hyperleptinemia

(A) Levels of circulating blood glucose (left), serum insulin (middle) and serum leptin (right) in 5-week male control (white, n = 5–8) and *Xrn1*-cKO (red, n = 5–6) mice.

(B and C) (C) To test leptin sensitivity, 5-week-old $Xrn1^{flox/flox}$ (black, n = 5) and *Xrn1*-cKO (red, n = 5) mice were intraperitoneally administered with leptin (5 μg/g body weight) every day for 5 days (blue arrows), daily body weight (B) and food intake (C) were measured for 11 days. Δbody weight (%) is shown as the percentage of daily weight gain normalized by daily body weight.

Figure 3. *Continued*

(D) Fed (left) and fasting (right) blood glucose levels in 5-, 7- and 9-week-old control (black, n = 5) and *Xrn1*-cKO (red, n = 5) mice are shown.

(E) Intraperitoneal glucose tolerance test (IPGTT) using 5-week-old control (black, n = 5) and *Xrn1*-cKO (red, n = 5) mice. Areas under the curves (AUC) of IPGTT are shown on the right side.

(F) Insulin tolerance test (ITT) using 5-week-old control (black, n = 5) and *Xrn1*-cKO (red, n = 5) mice. Values at 0 min are set as 100%. Areas under the curves (AUC) of ITT are shown on the right side. Data represent means ± SEM. Two-way ANOVA followed by Bonferroni post hoc test for fed and fasting blood glucose, IPGTT and ITT. Unpaired Student's t test for AUC, *$p < 0.05$; **$p < 0.01$; and ***$p < 0.001$. ns represents "not significant."

Xrn1-cKO mice. Weight gain, food intake and metabolic dysregulation such as impaired glucose tolerance and insulin resistance developed as early as 5 weeks old in *Xrn1*-cKO mice, before the onset of increased body weight.

Forebrain-specific disruption of *Xrn1* causes a metabolic shift and affects basal metabolism

To investigate whether the obese phenotype is caused by alterations in energy intake and/or energy expenditure, whole-body basal metabolism was examined by indirect calorimetry. Intriguingly, loss of XRN1 in the brain (central nervous system) caused an increase in respiratory exchange ratio (RER, VCO_2/VO_2; $p < 0.01$; Figure 4A), but little change in overall energy expenditure (kcal/kg/h; Figure 4B) at 6 weeks old, which corresponds to the onset of obesity. The value of the RER indicates the energy source: an RER of 1.0 indicates that only carbohydrates are used as an energy source, but if fat is the sole energy source the RER is 0.7 (Speakman, 2013). In control mice, RER oscillated during the day, with lower RER during the day indicating increased fat usage. In *Xrn1*-cKO mice, RER remained constant at around 1.0, indicating that these mice use only carbohydrates and suggesting that disruption of XRN1 function in neurons impairs the use of fat as an energy source in these mice. The RER was constant day and night in both 6-week-old and 12-week-old *Xrn1*-cKO mice, which is after the onset of obesity (Figure 4C). Nonetheless, energy expenditure was significantly decreased in these obese mice at 12 weeks old (day, $p < 0.01$; night, $p < 0.001$) (Figure 4D). To investigate whether reduced physical activity contributes to the decreased energy expenditure observed in *Xrn1*-cKO mice, locomotor activity was examined using a home-cage activity monitoring system. There was no difference in nocturnal activity, but diurnal activity appeared to decrease in *Xrn1*-cKO mice (Figure S4E). In summary, *Xrn1*-cKO mice do not exhibit the diurnal switch from carbohydrate to fat usage and expend less energy expenditure at 12 weeks old.

Xrn1-cKO mice exhibited upregulated expression of hypothalamic appetite and energy homeostasis-related genes in the hypothalamus

The hypothalamus regulates glucose homeostasis, leptin signaling, and energy expenditure by sensing hormones such as insulin and leptin, and by integrating and coordinating neurophysiological responses to regulate whole-body metabolism. To investigate the underlying cause of dysregulation of appetite and energy homeostasis in *Xrn1*-cKO mice, hypothalamic gene expression was examined by quantitative PCR (qPCR). Expression of mRNAs relevant to appetite and energy homeostasis was increased in the hypothalamus of *Xrn1*-cKO mice compared to control mice. These include mRNAs encoding *Agrp* and the inhibitors of the JAK-STAT and PI3K-AKT signaling pathways *Socs3*, *Ptp1b*, and *Tcptp* (Figure 5A).

As an exoribonuclease, XRN1 degrades mRNA and therefore XRN1 deletion could increase mRNA either directly, via reduced mRNA degradation, or indirectly via increased transcription. To clarify the effect of transcription, pre-mRNA expression was measured by qPCR. *Socs3* pre-mRNA was elevated in *Xrn1*-cKO hypothalamus, suggesting that transcription is increased. There was little change in *Agrp*, *Ptp1b*, and *Tcptp* pre-mRNAs, implying that the increase in these mRNAs in the *Xrn1*-cKO hypothalamus results from decreased mRNA degradation (Figure 5B). Western blotting revealed that protein expression of insulin receptor (INSR), SOCS3, PTP1B, and TCPTP were not altered in hypothalamus of 12-week-old *Xrn1*-cKO mice, whereas leptin receptor (LEPR) was significantly increased (Figures 5C and 5D), implying that dysregulated metabolism in *Xrn1*-cKO mice is not caused by changes of these genes. Since neither LEPR nor INSR was decreased in *Xrn1*-cKO hypothalamus, leptin resistance and insulin resistance in *Xrn1*-cKO mice were not caused by a lack of LEPR or INSR. Moreover, immunohistochemistry showed an increase in AgRP protein in the arcuate nucleus of the hypothalamus (ARC) of *Xrn1*-cKO mice compared to control mice (Figures 5E and 5F). Increased AgRP in *Xrn1*-cKO hypothalamus could contribute to the obese phenotype with elevated appetite, leptin resistance, decreased energy expenditure, hyperglycemia, and insulin resistance (Figure 6).

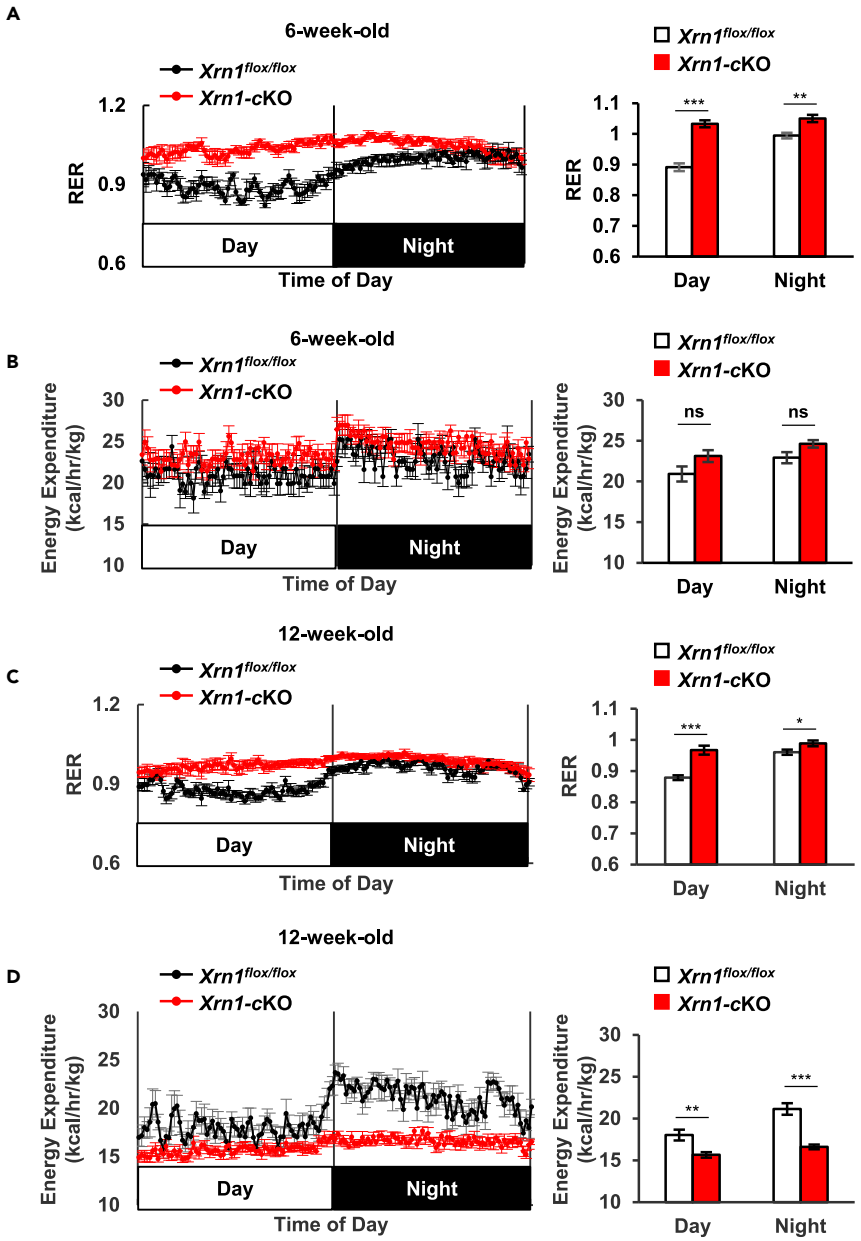

Figure 4. *Xrn1*-cKO mice displayed increased VCO_2 and energy expenditure and constant RER, indicating an inability to utilize fat as an energy source

(A and B) (A) respiratory exchange ratio (RER) and (B) energy expenditure of male 6-week-old *Xrn1*$^{flox/flox}$ mice (black, n = 5) and *Xrn1*-cKO mice (red, n = 6) were measured. RER is calculated by VCO_2/VO_2. An RER of 1.0 means that carbohydrates are the dominant energy source; 0.7 indicates that fat is the dominant energy source.

(C and D) (C) Respiratory exchange ratio (RER) and (D) energy expenditure of male 12-week-old *Xrn1*$^{flox/flox}$ mice (black, n = 8) and *Xrn1*-cKO mice (red, n = 8) were measured. Average values of each parameter in *Xrn1*$^{flox/flox}$ mice (white) and *Xrn1*-cKO mice (red) during light and dark are shown on the right sides.

DISCUSSION

In eukaryotes, XRN1 catalyzes the last step of mRNA degradation after deadenylation and decapping. Regulation of mRNA turnover is crucial for development and homeostasis in various mammalian tissues. Mice that lack components of the mRNA degradation machinery exhibit different types of physiological dysregulation, such as metabolic disorders and male infertility (Morita et al., 2011; Takahashi et al., 2015;

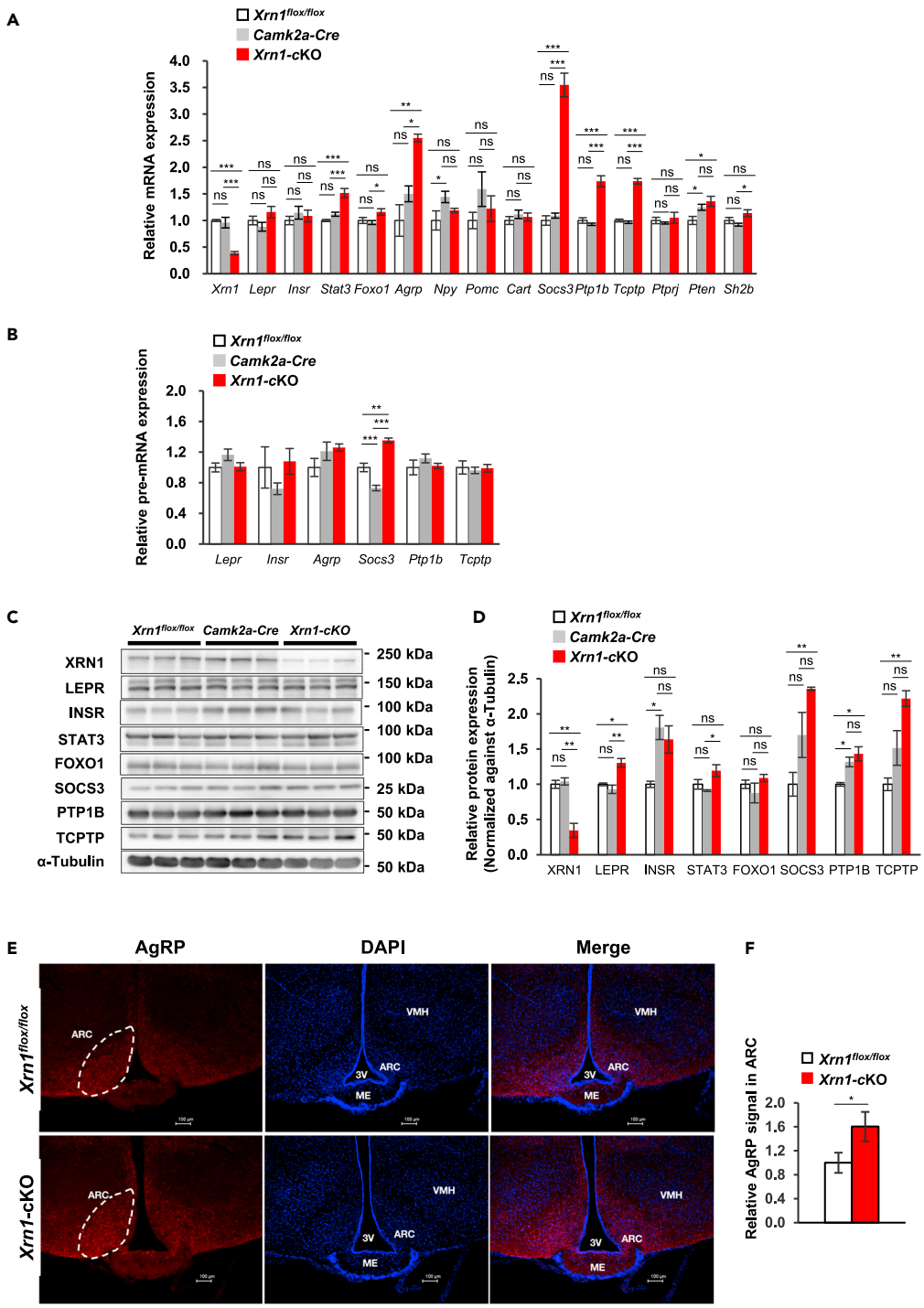

Figure 5. *Xrn1*-cKO mice exhibit upregulated appetite and energy homeostasis-related genes in the hypothalamus

(A) Quantitative PCR (qPCR) analysis of the indicated mRNA levels in the hypothalamus of 10- to 14-week-old control (*Xrn1*$^{flox/flox}$: white, n = 5; *Camk2a-Cre*: gray, n = 10) and *Xrn1*-cKO mice (red, n = 5). The value of the average of *Xrn1*$^{flox/flox}$ mice was set as 1. Data represent means ± SEM. One-way ANOVA, Tukey post hoc test, *p < 0.05; **p < 0.01; and ***p < 0.001.

(B) qPCR analysis of the indicated pre-mRNAs in the hypothalamus of 10- to 14-week-old control (*Xrn1*$^{flox/flox}$: white, n = 5; *Camk2a-Cre*: gray, n = 10) and *Xrn1*-cKO mice (red, n = 5). The average value of *Xrn1*$^{flox/flox}$ mice was set as 1. Data represent means ± SEM. One-way ANOVA, Tukey post hoc test, *p < 0.05; **p < 0.01; and ***p < 0.001.

Figure 5. *Continued*

(C) Protein expression of XRN1, LERP, INSR, STAT3, FOXO1, SOCS3, PTP1B, TCPTP, and α-Tubulin in 12-week-old control (*Xrn1*$^{flox/flox}$: white, n = 3; *Camk2a-Cre*: gray, n = 3) and *Xrn1*-cKO mice (red, n = 3).

(D) Quantitative analysis of protein bands in panel 5C. Band intensities were measured using NIH ImageJ. Values of the average of *Xrn1*$^{flox/flox}$ mice were set as 1. Data represent means ± SEM. One-way ANOVA, Tukey post hoc test, *$p < 0.05$; **$p < 0.01$; and ***$p < 0.001$.

(E) Immunofluorescence analysis of AgRP (red) and nuclei by counterstaining with DAPI (blue) in the ARC of *Xrn1*-cKO and control (*Xrn1*$^{flox/flox}$) mice at 12 weeks old.

(F) Quantification of the AgRP signal in the ARC of *Xrn1*-cKO (red) and control (white) mice.

Nakamura et al., 2004). Those studies focused on regulation of deadenylation by the CCR4-NOT complex at the 3′ end of mRNA, which is an early step of mRNA degradation. This study is the first to reveal the physiological function of XRN1, a 5′–3′ exoribonuclease, using conditional knockout mice that exhibit obesity with hyperphagia. XRN1 protein expression is increased in 20-week-old wild-type mice fed with a high-fat diet for 12 weeks (Figures S6A and S6B). Based on our study, increased XRN1 may be expected to reduce feeding and increase the use of fat as an energy source. Moreover, *Xrn1* mRNA was also increased by fasting in 10-week-old control (*Xrn1*$^{flox/flox}$) mice (Figure S6C). Therefore, XRN1 expression is responsive to perturbations to food intake and energy balance, which may contribute to the regulation of these processes to maintain metabolic homeostasis. Expression of metabolic genes in the hypothalamus of *Xrn1*-cKO mice is altered, implying that RNA degradation is critical not only in peripheral tissues, but also in the central nervous system to maintain homeostasis of metabolism-related gene expression.

Our unpublished data using *Camk2a-Cre* conditional KO mice demonstrate that forebrain-specific knockout of *Cnot1* or *Cnot3*, encoding a scaffold protein and a regulatory subunit of the CCR4-NOT complex, respectively, is embryonic lethal, implying that regulation of mRNA degradation by the CCR4-NOT complex in embryonic neurons is essential. On the other hand, *Xrn1*-cKO mice are viable, suggesting that the last step of mRNA degradation by XRN1 in neurons is less critical during embryogenesis. This attenuated phenotype caused by the lack of XRN1 might also be because of the fact that XRN1 targets specific transcripts, rather than bulk mRNAs (Souret et al., 2004; Rymarquis et al., 2011). Further studies should identify transcripts specifically targeted by XRN1 that are essential for embryogenesis and neuronal functions.

The ribonuclease Dicer processes miRNA precursors into functional miRNAs, and conditional *Dicer* knockout mice in anorexigenic pro-opiomelanocortin (POMC) neurons exhibit obesity with hyperphagia, steatosis, impaired glucose metabolism, and hyperleptinemia (Schneeberger et al., 2012), demonstrating the importance of miRNA-mediated gene expression in regulation of whole-body metabolic homeostasis. XRN1 is also thought to participate in miRNA-mediated decay (Zangari et al., 2017). Our current study demonstrates that mRNAs that contribute to metabolism are regulated by XRN1 in the hypothalamus (Figure 5A), and this could be mediated by miRNAs. We provide evidence that forebrain-specific knockout of the 5′–3′ exoribonuclease XRN1 causes obesity with hyperphagia, which results in hyperglycemia, hyperinsulinemia and hyperleptinemia. Taken together, these findings revealed the importance of XRN1-mediated mRNA degradation in regulating gene expression in the leptin signaling pathway.

Hyperleptinemia is often observed in obese mouse models. Under normal conditions, increased adiposity leads to more leptin production. Increased circulating leptin levels are detected by the hypothalamus and cause metabolic shifts to achieve energy homeostasis. However, obese individuals are less sensitive to leptin, and resistant to anorexigenic effects of leptin, a state called "leptin resistance" (St-Pierre and Tremblay, 2012). Previous studies have shown that leptin resistance is caused by various mechanisms, such as ER stress, inflammation, and attenuation of leptin signaling by SOCS3 and protein tyrosine phosphatases such as PTP1B and TCPTP (Bjørbæk et al., 1998; Loh et al., 2011; St-Pierre and Tremblay, 2012; Tanti et al., 2013; White et al., 2009; Zhang et al., 2008). *Xrn1*-cKO mice are obese with high serum leptin levels (Figures 3A, S2A, and S2B). In addition, *Xrn1*-cKO mice develop leptin resistance before the onset of obesity (Figures 3B and 3C), which may be caused by increased *Socs3*, *Ptp1b* and *Tcptp* mRNAs in *Xrn1*-cKO hypothalamus (Figure 5A). It is also possible that upregulation of leptin resistance mRNAs may be a consequence of obesity, rather than its cause. For instance, *Socs3* overexpression in leptin receptor-expressing neurons results in a lean phenotype rather than obesity (Reed et al., 2010). In addition, AgRP neuron-specific *Socs3* overexpression does not cause obesity, but instead leads to a phenotype similar to that caused by short-term consumption of a high-fat diet (Olofsson et al., 2013). POMC neuron-specific

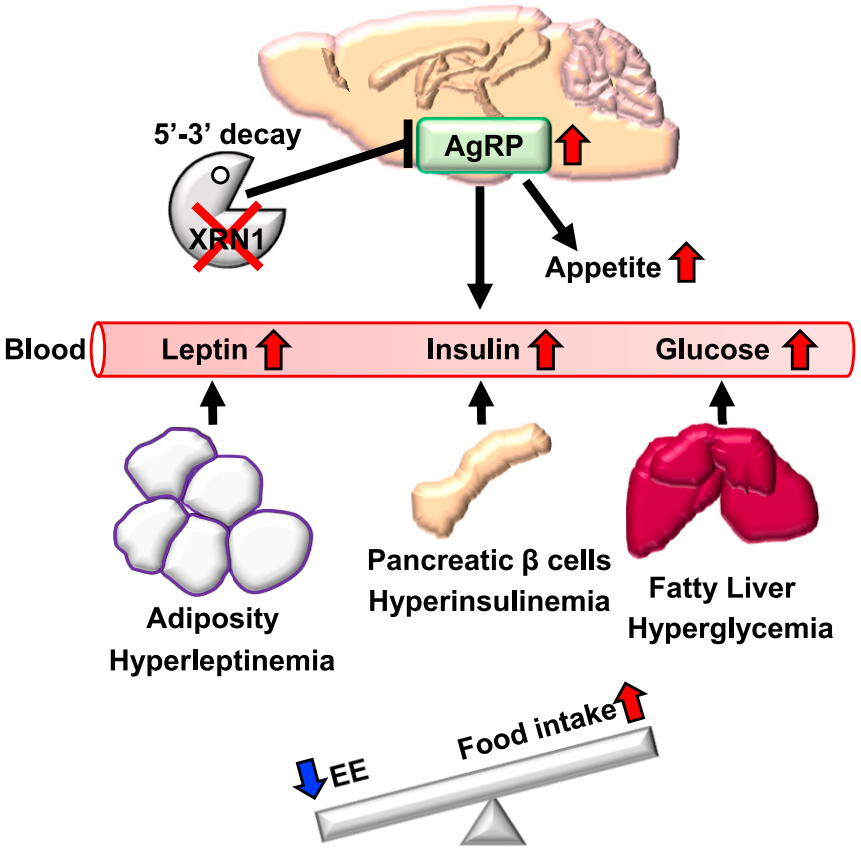

Figure 6. A lack of XRN1 in neurons causes increased appetite, decreased energy expenditure, hyperglycemia, and dysfunctions of metabolic hormones

Appetite circuits in the hypothalamus and consequent metabolic functions in peripheral tissues such as adipose tissue, pancreas, and liver. The diagram indicates dysregulation of metabolic homeostasis by activated AgRP neurons in *Xrn1*-cKO hypothalamus. EE: Energy expenditure.

Socs3 overexpression causes obesity without severe weight gain and hyperphagia (Reed et al., 2010). Therefore, upregulation of *Socs3* mRNA is unlikely to be the primary cause of the phenotypes observed in *Xrn1*-cKO mice.

Xrn1-cKO mice are not only obese, but their bodies are longer than those of littermates (Figures 1C and 1D). Interestingly, *ob*/*ob* and *db*/*db* mice do not exhibit increased body length. Instead, they are shorter than their littermates (Dubuc, 1976; Graham et al., 1997). On the other hand, *Agrp*-overexpressing mutant mice, *Pomc*-knockout mice, *Mc4r*-knockout mice, and *MC4R*-deficient human patients exhibit longer body length (Farooqi et al., 2003; Graham et al., 1997; Huszar et al., 1997; Ollmann et al., 1997; Yaswen et al., 1999), which could indicate that phenotypes of *Xrn1*-cKO mice are related to hyperactive melanocortin signaling.

RER in $Xrn1^{flox/flox}$ mice is lower during the day and higher at night, reflecting the diurnal metabolic shift from fat to carbohydrate usage. In contrast, *Xrn1*-cKO mice exhibited constant RER during both day and night, indicating that carbohydrates are the dominant source of energy throughout the day (Figures 4A and 4C). A recent study revealed that activation of AgRP neurons affects substrate utilization in favor of carbohydrate use over lipid use (Cavalcanti-de-Albuquerque et al., 2019), demonstrating that AgRP neurons regulate lipogenesis and glycolysis in white adipose tissue via sympathetic signaling. In consequence, activation of AgRP neurons leads to an increase in RER. We hypothesize that the loss of XRN1 may lead to activation of AgRP neurons in *Xrn1*-cKO mice, as the phenotype is similar to *Agrp*-overexpressing mice (Graham et al., 1997). Because leptin acts primarily via AgRP neurons to regulate body weight and

food intake (Xu et al., 2018), it is feasible that leptin resistance in *Xrn1*-cKO mice might originate from activated AgRP neurons. It is unlikely that the increase in *Agrp* mRNA in *Xrn1*-cKO mice results directly from a loss of XRN1 since AgRP neurons are GABAergic (Horvath et al., 1997), and *Camk2a-Cre* expression is almost exclusively restricted to glutamatergic neurons (Wang et al., 2013). AgRP neurons are directly activated by excitatory glutamatergic TRH-/PACAP-positive neurons located in the paraventricular nucleus of the hypothalamus (PVH) (Krashes et al., 2014). This neuronal pathway drives feeding and if these neurons are overactive in *Xrn1*-cKO brain, it provides a possible mechanism by which loss of XRN1 in glutamatergic neurons could lead to activation of GABAergic AgRP neurons. Activation of AgRP neurons via this pathway was able to drive feeding even in sated mice and therefore it could override satiety signals such as increased leptin and lead to leptin resistance.

Previous studies have shown that XRN1 regulates target gene expression by controlling mRNA stability, transcription, and translation (Braun and Young, 2014; Luchelli et al., 2015). Therefore, further comprehensive analyses are required to fully clarify mechanisms of activated AgRP neurons in *Xrn1*-cKO mice. Communication between the central nervous system and peripheral metabolic tissues is important to determine whole-body energy metabolism (Myers and Olson, 2012). Further analyses of peripheral tissues are required to determine whether the metabolic alterations in *Xrn1*-cKO mice are due to dysregulation of lipogenesis and glycolysis.

RNA modifications such as N^6-methyladenosine (m^6A) are increasingly recognized as being important in gene expression. XRN1 interacts with YT521-B homology domain-containing 2 (YTHDC2), an m^6A reader that recognizes internal RNA modifications in mRNAs and is indispensable for male and female fertility (Wojtas et al., 2017; Hsu et al., 2017). N6-adenosine methylation in RNA is mediated by YTH domain family proteins (YTHDF1, YTHDF2, and YTHDF3) and YTH domain-containing proteins (YTHDC1 and YTHDC2), each of which serves a distinctive physiological function. YTHDF1 and YTHDF3 contribute to mRNA translation, whereas YTHDF2 enhances mRNA decay in processing bodies via recruitment of the CCR4-NOT complex (Du et al., 2016). Although YTHDC1 regulates pre-mRNA splicing, little is known about the physiological function of YTHDC2, beyond its RNA helicase activity. The physiological relevance of the interaction between XRN1 and YTHDC2 is not clear. YTHDC2 is ubiquitously expressed in various tissues, including the hypothalamus. Aberrant recognition of RNA modifications, because of the lack of association between XRN1 and YTHDC2 in the hypothalamus of *Xrn1*-cKO mice may contribute to metabolic disorders. Further study is required to determine the role of XRN1 in gene regulation by RNA modification.

In conclusion, we demonstrated that forebrain-specific *Xrn1* knockout causes defects in energy homeostasis and leads to obesity and hyperphagia. Although XRN1 is thought to degrade bulk mRNAs in principle, *Xrn1*-cKO mice exhibit very specific phenotypes, implying that XRN1 targets specific mRNAs under certain circumstances. Moreover, gene expression of appetite and energy homeostasis-related genes in the hypothalamus of *Xrn1*-cKO mice suggests that either 5′–3′ decay targets particular mRNAs or the majority of the 5′–3′ decay targets are degraded by different decay pathways, such as 3′-5′ decay in *Xrn1*-cKO mice. In summary, understanding the molecular mechanisms of obesity and energy homeostasis regulated by XRN1 may enable development of novel therapeutic strategies for metabolic disorders such as obesity and diabetes.

Limitations of the study

Camk2a-Cre mice were used for our study; hence we could not conclude which specific neural cells are responsible for the dysregulated appetite in *Xrn1*-cKO mice. Targeting specific populations of neurons using, for example, *Pomc-Cre, Agrp-Cre, PACAP-Cre, and/or TRH-Cre* mice to generate *Xrn1*-cKO mice would clarify in which neurons the dysregulated gene expression caused by the deletion of *Xrn1* contributes to aberrant appetite.

STAR★METHODS

Detailed methods are provided in the online version of this paper and include the following:

- KEY RESOURCES TABLE
- RESOURCE AVAILABILITY
  - Lead contact

SUPPLEMENTAL INFORMATION

Supplemental information can be found online at https://doi.org/10.1016/j.isci.2021.103151.

ACKNOWLEDGMENTS

This work was supported by the Okinawa Institute of Science and Technology (OIST) subsidiary budget to TY. AT and AY were supported by a Grant-in-Aid for Scientific Research (C) (17K07292 and 18K06975, respectively) and a Grant-in-Aid for Scientific Research on Innovative Areas (17H06018 and 20H05351, respectively), from the Japan Ministry of Education, Culture, Sports, Science and Technology. PS was supported by a Grant-in-Aid for Young Scientist (18K16218). We thank OIST for generous support to the Cell Signal Unit.

AUTHOR CONTRIBUTIONS

ST, AT, PS, AY and TY designed the study. ST, HMAM, AY, and RH performed experiments. TA and KI generated *Xrn1* conditional knockout mice. AT and PS provided experimental advice and assistance. ST, AY, PS and TY wrote the manuscript.

DECLARATION OF INTERESTS

The authors declare no competing interests.

Received: March 23, 2021
Revised: July 10, 2021
Accepted: September 16, 2021
Published: October 22, 2021

REFERENCES

Audic, Y., and Hartley, R.S. (2004). Post-transcriptional regulation in cancer. Biol. Cell *96*, 479–498.

Bjørbæk, C., Elmquist, J.K., Frantz, J.D., Shoelson, S.E., and Flier, J.S. (1998). Identification of SOCS-3 as a potential mediator of central leptin resistance. Mol. Cell *1*, 619–625.

Braun, K.A., and Young, E.T. (2014). Coupling mRNA synthesis and decay. Mol. Cell. Biol. *34*, 4078–4087.

Casanova, E., Fehsenfeld, S., Mantamadiotis, T., Lemberger, T., Greiner, E., Stewart, A.F., and Schutz, G. (2001). A CamKIIalpha iCre BAC allows brain-specific gene inactivation. Genesis *31*, 37–42.

Cavalcanti-de-Albuquerque, J., Bober, J., Zimmer, M.R., and Dietrich, M.O. (2019). Regulation of substrate utilization and adiposity by Agrp neurons. Nat. Commun. *10*, 311.

Chen, C.Y.A., and Shyu, A.B. (2011). Mechanisms of deadenylation-dependent decay. Wiley Interdiscip. Rev. RNA *2*, 167–183.

Du, H., Zhao, Y., He, J., Zhang, Y., Xi, H., Liu, M., Ma, J., and Wu, L. (2016). YTHDF2 destabilizes m(6)A-containing RNA through direct recruitment of the CCR4-NOT deadenylase complex. Nat. Commun. *7*, 12626.

Dubuc, P.U. (1976). The development of obesity, hyperinsulinemia, and hyperglycemia in ob/ob mice. Metab. Clin. Exp. *25*, 1567–1574.

Farooqi, I.S., Keogh, J.M., Yeo, G.S.H., Lank, E.J., Cheetham, T., and O'Rahilly, S. (2003). Clinical spectrum of obesity and mutations in the melanocortin 4 receptor gene. New Engl. J. Med. *348*, 1085–1095.

Garneau, N.L., Wilusz, J., and Wilusz, C.J. (2007). The highways and byways of mRNA decay. Nat. Rev. Mol. Cell Biol. *8*, 113–126.

Graham, M., Shutter, J.R., Sarmiento, U., Sarosi, I., and Stark, K.L. (1997). Overexpression of Agrt leads to obesity in transgenic mice. Nat. Genet. *17*, 273–274.

Grima, D., Sullivan, M., Zabolotskaya, M., Browne, C., Seago, J., Wan, K.C., Okada, Y., and Newbury, S. (2008). The 5′–3′ exoribonuclease pacman is

required for epithelial sheet sealing in Drosophila and genetically interacts with the phosphatase puckered. Biol. Cell *100*, 687–701.

Horvath, T.L., Bechmann, I., Naftolin, F., Kalra, S.P., and Leranth, C. (1997). Heterogeneity in the neuropeptide Y-containing neurons of the rat arcuate nucleus: GABAergic and non-GABAergic subpopulations. Brain Res. *756*, 283–286.

Hsu, P.J., Zhu, Y., Ma, H., Guo, Y., Shi, X., Liu, Y., Qi, M., Lu, Z., Shi, H., Wang, J., et al. (2017). Ythdc2 is an N(6)-methyladenosine binding protein that regulates mammalian spermatogenesis. Cell Res. *27*, 1115–1127.

Huszar, D., Lynch, C.A., Fairchild-Huntress, V., Dunmore, J.H., Fang, Q., Berkemeier, L.R., Gu, W., Kesterson, R.A., Boston, B.A., Cone, R.D., et al. (1997). Targeted disruption of the melanocortin-4 receptor results in obesity in mice. Cell *88*, 131–141.

Jones, C.I., Zabolotskaya, M.V., and Newbury, S.F. (2012). The 5′ → 3′ exoribonuclease XRN1/Pacman and its functions in cellular processes and development. Wiley Interdiscip. Rev. RNA *3*, 455–468.

Krashes, M.J., Shah, B.P., Madara, J.C., Olson, D.P., Strochlic, D.E., Garfield, A.S., Vong, L., Pei, H., Watabe-Uchida, M., Uchida, N., et al. (2014). An excitatory paraventricular nucleus to AgRP neuron circuit that drives hunger. Nature *507*, 238–242.

Larimer, F.W., and Stevens, A. (1990). Disruption of the gene XRN1, coding for a 5′——3′ exoribonuclease, restricts yeast cell growth. Gene *95*, 85–90.

Lin, M.-D., Jiao, X., Grima, D., Newbury, S.F., Kiledjian, M., and Chou, T.-B. (2008). Drosophila processing bodies in oogenesis. Dev. Biol. *322*, 276–288.

Linder, B., Fischer, U., and Gehring, N.H. (2015). mRNA metabolism and neuronal disease. FEBS Lett. *589*, 1598–1606.

Loh, K., Fukushima, A., Zhang, X., Galic, S., Briggs, D., Enriori, P.J., Simonds, S., Wiede, F., Reichenbach, A., Hauser, C., et al. (2011). Elevated hypothalamic TCPTP in obesity contributes to cellular leptin resistance. Cell Metab. *14*, 684–699.

Luchelli, L., Thomas, M.G.G., and Boccaccio, G.L. (2015). Synaptic control of mRNA translation by reversible assembly of XRN1 bodies. J. Cell Sci. *128*, 1542–1554.

Mang, G.M., Pradervand, S., Du, N.-H., Arpat, A., Preitner, F., Wigger, L., Gatfield, D., and Franken, P. (2015). A neuron-specific deletion of the MicroRNA-processing enzyme DICER induces severe but transient obesity in mice. PLoS One *10*, e0116760.

Morita, M., Oike, Y., Nagashima, T., Kadomatsu, T., Tabata, M., Suzuki, T., Nakamura, T., Yoshida, N., Okada, M., and Yamamoto, T. (2011). Obesity resistance and increased hepatic expression of catabolism-related mRNAs in Cnot3+/- mice. EMBO J. *30*, 4678–4691.

Mostafa, D., Yanagiya, A., Georgiadou, E., Wu, Y., Stylianides, T., Rutter, G.A., Suzuki, T., and Yamamoto, T. (2020). Loss of β-cell identity and diabetic phenotype in mice caused by disruption of CNOT3-dependent mRNA deadenylation. Commun. Biol. *3*, 476.

Myers, M.G., Jr., and Olson, D.P. (2012). Central nervous system control of metabolism. Nature *491*, 357–363.

Nakamura, T., Yao, R., Ogawa, T., Suzuki, T., Ito, C., Tsunekawa, N., Inoue, K., Ajima, R., Miyasaka, T., Yoshida, Y., et al. (2004). Oligo-astheno-teratozoospermia in mice lacking Cnot7, a regulator of retinoid X receptor beta. Nat. Genet. *36*, 528–533.

Newbury, S., and Woollard, A. (2004). The 5′–3′ exoribonuclease xrn-1 is essential for ventral epithelial enclosure during *C. elegans* embryogenesis. RNA *10*, 59–65.

Ollmann, M.M., Wilson, B.D., Yang, Y.-K., Kerns, J.A., Chen, Y., Gantz, I., and Barsh, G.S. (1997). Antagonism of central melanocortin receptors in vitro and in vivo by Agouti-related protein. Science *278*, 135–138.

Olofsson, L.E., Unger, E.K., Cheung, C.C., and Xu, A.W. (2013). Modulation of AgRP-neuronal function by SOCS3 as an initiating event in diet-induced hypothalamic leptin resistance. Proc. Natl. Acad. Sci. *110*, E697–E706.

Reed, A.S., Unger, E.K., Olofsson, L.E., Piper, M.L., Myers, M.G., and Xu, A.W. (2010). Functional role of suppressor of cytokine signaling 3 upregulation in hypothalamic leptin resistance and long-term energy homeostasis. Diabetes *59*, 894–906.

Rymarquis, L.A., Souret, F.F., and Green, P.J. (2011). Evidence that XRN4, an Arabidopsis homolog of exoribonuclease XRN1, preferentially impacts transcripts with certain sequences or in particular functional categories. RNA *17*, 501–511.

Sakai, K., and Miyazaki, J. (1997). A transgenic mouse line that retains Cre recombinase activity in mature oocytes irrespective of the cre transgene transmission. Biochem. Biophys. Res. Commun. *237*, 318–324.

Schneeberger, M., Altirriba, J., Garcia, A., Esteban, Y., Castano, C., Garcia-Lavandeira, M., Alvarez, C.V., Gomis, R., and Claret, M. (2012). Deletion of miRNA processing enzyme Dicer in POMC-expressing cells leads to pituitary dysfunction, neurodegeneration and development of obesity. Mol. Metab. *2*, 74–85.

Schneider, C.A., Rasband, W.S., and Eliceiri, K.W. (2012). NIH Image to ImageJ: 25 years of image analysis. Nat. Methods *9*, 671–675.

Souret, F.F., Kastenmayer, J.P., and Green, P.J. (2004). AtXRN4 degrades mRNA in Arabidopsis and its substrates include selected miRNA targets. Mol. Cell *15*, 173–183.

Speakman, J.R. (2013). Measuring energy metabolism in the mouse - theoretical, practical, and analytical considerations. Front. Physiol. *4*, 34.

St-Pierre, J., and Tremblay, M.L. (2012). Modulation of leptin resistance by protein tyrosine phosphatases. Cell Metab. *15*, 292–297.

Suzuki, T., Kikuguchi, C., Nishijima, S., Nagashima, T., Takahashi, A., Okada, M., and Yamamoto, T. (2019). Postnatal liver functional maturation requires Cnot complex-mediated decay of mRNAs encoding cell cycle and immature liver genes. Development *146*, dev168146.

Takahashi, A., Adachi, S., Morita, M., Tokumasu, M., Natsume, T., Suzuki, T., and Yamamoto, T. (2015). Post-transcriptional stabilization of Ucp1 mRNA protects mice from diet-induced obesity. Cell Rep. *13*, 2756–2767.

Takahashi, A., Suzuki, T., Soeda, S., Takaoka, S., Kobori, S., Yamaguchi, T., Mohamed, H., Yanagiya, A., Abe, T., Shigeta, M., et al. (2020). The CCR4-NOT complex maintains liver homeostasis through mRNA deadenylation. Life Sci. alliance *3*, e201900494.

Takahashi, A., Takaoka, S., Kobori, S., Yamaguchi, T., Ferwati, S., Kuba, K., Yamamoto, T., and Suzuki, T. (2019). The CCR4–NOT deadenylase complex maintains adipocyte identity. Int. J. Mol. Sci. *20*, 5274.

Tanti, J.-F., Ceppo, F., Jager, J., Berthou, F., Tanti, J.-F., Ceppo, F., Jager, J., and Berthou, F. (2013). Implication of inflammatory signaling pathways in obesity-induced insulin resistance. Front. Endocrinol. *3*, 181.

Taylor, S.C., Nadeau, K., Abbasi, M., Lachance, C., Nguyen, M., and Fenrich, J. (2019). The ultimate qPCR experiment: producing publication quality, reproducible data the first time. Trends Biotechnol. *37*, 761–774.

Timper, K., and Brüning, J.C. (2017). Hypothalamic circuits regulating appetite and energy homeostasis: pathways to obesity. Dis. Models Mech. *10*, 679–689.

Wang, X., Zhang, C., Szabo, G., and Sun, Q.Q. (2013). Distribution of CaMKIIalpha expression in the brain in vivo, studied by CaMKIIalpha-GFP mice. Brain Res. *1518*, 9–25.

White, C.L., Whittington, A., Barnes, M.J., Wang, Z., Bray, G.A., and Morrison, C.D. (2009). HF diets increase hypothalamic PTP1B and induce leptin resistance through both leptin-dependent and -independent mechanisms. Am. J. Physiol.-Endocrinol. Metab. *296*, E291–E299.

Wojtas, M.N., Pandey, R.R., Mendel, M., Homolka, D., Sachidanandam, R., and Pillai, R.S. (2017). Regulation of m(6)A transcripts by the 3′→5′ RNA helicase YTHDC2 is essential for a successful meiotic program in the mammalian germline. Mol. Cel. *68*, 374–1971793920.

Xu, J., Bartolome, C.L., Low, C.S., Yi, X., Chien, C.H., Wang, P., and Kong, D. (2018). Genetic identification of leptin neural circuits in energy and glucose homeostases. Nature *556*, 505–509.

Yamaguchi, T., Suzuki, T., Sato, T., Takahashi, A., Watanabe, H., Kadowaki, A., Natsui, M., Inagaki, H., Arakawa, S., Nakaoka, S., et al. (2018). The CCR4-NOT deadenylase complex controls Atg7-dependent cell death and heart function. Sci. Signal. *11*, eaan3638.

Yaswen, L., Diehl, N., Brennan, M.B., and Hochgeschwender, U. (1999). Obesity in the

mouse model of pro-opiomelanocortin deficiency responds to peripheral melanocortin. Nat. Med. *5*, 1066–1070.

Zabolotskaya, M.V., Grima, D.P., Lin, M.-D.D., Chou, T.-B.B., and Newbury, S.F. (2008). The 5′–3′ exoribonuclease Pacman is required for normal male fertility and is dynamically localized in cytoplasmic particles in Drosophila testis cells. Biochem. J. *416*, 327–335.

Zangari, J., Ilie, M., Rouaud, F., Signetti, L., Ohanna, M., Didier, R., Romeo, B., Goldoni, D., Nottet, N., Staedel, C., et al. (2017). Rapid decay of engulfed extracellular miRNA by XRN1 exonuclease promotes transient epithelial-mesenchymal transition. Nucleic Acids Res. *45*, 4131–4141.

Zhang, X., Zhang, G., Zhang, H., Karin, M., Bai, H., and Cai, D. (2008). Hypothalamic IKKβ/NF-κB and ER stress link overnutrition to energy imbalance and obesity. Cell *135*, 61–73.

STAR★METHODS

KEY RESOURCES TABLE

REAGENT or RESOURCE	SOURCE	IDENTIFIER
Antibodies		
Rabbit polyclonal anti-XRN1	Bethyl Laboratories	Cat#A300-443A; RRID: AB_2219047
Rabbit monoclonal anti-Leptin Receptor	Abcam	Cat#ab177469
Rabbit monoclonal anti-Insulin Receptor	Cell Signaling	Cat#3025; RRID: AB_2280448
Rabbit monoclonal anti-Stat3 (79D7)	Cell Signaling	Cat#4904; RRID: AB_331269
Rabbit monoclonal anti-FoxO1 (C29H4)	Cell Signaling	Cat#2880; RRID: AB_2106495
Rabbit polyclonal anti-SOCS3	Cell Signaling	Cat#2923; RRID: AB_2255132
Rabbit polyclonal anti-PTP1B	Proteintech	Cat# 11334-1-AP; RRID: AB_10642566
Rabbit monoclonal anti-TCPTP (TC45) (D7T7D)	Cell Signaling	Cat#58935; RRID: AB_2799550
Rabbit polyclonal anti-UCP1	Abcam	Cat#ab10983; RRID: AB_2241462
Rabbit polyclonal anti-AgRP	Phoenix Pharmaceuticals	Cat# H-003-57; RRID: AB_2313909
Mouse monoclonal anti-CNOT1, Bio Matrix, #1012	This paper	N/A
Rabbit monoclonal anti-CNOT2	Cell Signaling	Cat#34214; RRID: AB_2799049
Mouse monoclonal anti-CNOT3, Bio Matrix, #54	This paper	N/A
Mouse monoclonal anti-CNOT7	Abnova	Cat#H00029883-M01; RRID: AB_606077
Rabbit monoclonal anti-α-tubulin	Sigma-Aldrich	Cat#T9026; RRID: AB_477593
Rabbit monoclonal anti-GAPDH (14C10)	Cell Signaling	Cat# 2118; RRID: AB_561053
Rabbit monoclonal anti-β-Actin (13E5)	Cell Signaling	Cat# 4970; RRID: AB_2223172
Sheep monoclonal anti-Mouse IgG - Horseradish Peroxidase antibody	GE Healthcare	Cat#NA931; RRID: AB_772210
Donkey anti-Rabbit IgG, Whole Ab ECL Antibody, HRP Conjugated	GE Healthcare	Cat#NA934; RRID: AB_772206
Goat polyclonal anti-Rabbit IgG H&L (Alexa Fluor 555)	Abcam	Cat#ab150078; RRID: AB_2722519
Chemicals, peptides, and recombinant proteins		
Leptin	R&D Systems	Cat#498-OB
Insulin	Eli Lilly	Cat#Humalog
Critical commercial assays		
Mouse Leptin ELISA kit	Abcam	Cat#ab199082
Mouse Insulin ELISA kit	Mercodia	Cat#10-1247-01
VECTASTAIN ABC HRP Kit (Peroxidase, Rabbit IgG)	Vector Laboratories	PK-4001
Experimental models: Organisms/strains		
Mouse: *Xrn1* $^{flox/+}$	This paper	NA
Mouse: B6.FVB-Tg(Camk2a-cre)2Gsc/Cnrm	Casanova et al. (2001)	EM:01153 at EMMA; https://www.infrafrontier.eu/
Mouse: C57BL/6J	CLEA Japan	Cat#C57BL/6JJcl
Oligonucleotides		
Primers for gRNA and ssODN to generate *Xrn1*$^{flox/+}$ mice, see Table S1	This paper	N/A
Primers for genotyping, see Table S2	This paper	N/A

(*Continued on next page*)

Continued

REAGENT or RESOURCE	SOURCE	IDENTIFIER
Primers for qPCR, see Table S3	This paper	N/A
Primers for qPCR to detect pre-mRNAs, see Table S4	This paper	N/A
Software and algorithms		
ImageJ	Schneider et al. (2012)	https://imagej.nih.gov/ij/
R software	The R foundation	R version 3.6.1
GraphPad Prism	GraphPad Software, Inc	Versions 8.0.2
Other		
High fat diet	CLEA Japan	Cat#HFD32
Normal diet	CLEA Japan	Cat#NCD, CA1

RESOURCE AVAILABILITY

Lead contact

Further information and requests for resources and reagents should be directed to and will be fulfilled by the Lead Contact, Tadashi Yamamoto (tadashi.yamamoto@oist.jp).

Materials availability

Mouse line (*Xrn1*$^{flox/+}$) generated in this study has been deposited to the Laboratory for Animal Resources and Genetic Engineering, RIKEN Center for Biosystems Dynamics Research.

Data and code availability

- All data reported in this paper will be shared by the lead contact upon request.
- This paper does not report original code.
- Any additional information required to reanalyze the data reported in this paper is available from the lead contact upon request.

EXPERIMENTAL MODEL AND SUBJECT DETAILS

Mice

Xrn1$^{flox/+}$ mice were generated by single-strand oligodeoxynucleotide (ssODN)-mediated knock-in with CRISPR-Cas system using C57BL/6N zygotes, in which *loxP* sites flank exons 2 and 6 of the *Xrn1* gene (accession no. CDB0007E: http://www2.clst.riken.jp/arg/micelist.html) (Figure S1A). Two guide RNAs (gRNAs) and ssODN targeting introns 1 and 6 of the *Xrn1* gene and Cas9 were injected into wild-type zygotes. gRNA and ssODN sequences are listed in Table S1. The *loxP* insertion in *cis* orientation was confirmed by genotyping in F1 offspring. Primers used for detection of wild-type and floxed alleles are listed in Table S2. *CAG-Cre* mice, which express the Cre recombinase gene under control of the cytomegalovirus immediate early enhancer-chicken beta-actin hybrid (CAG) promoter (Sakai and Miyazaki, 1997), were used to generate whole-body knockout mice of *Xrn1*. To generate whole-body knockout mice of *Xrn1*, we crossed *Xrn1*$^{flox/flox}$ mice with *CAG-Cre*$^{cre/+}$ mice. Primers used for detection of wild-type, floxed, and knockout alleles are listed in Table S2.

Camk2a-Cre mice (B6.FVB-Tg(Camk2a-cre)2Gsc/Cnrm), which express the Cre recombinase gene under control of the promoter of mouse calcium/calmodulin-dependent protein kinase II alpha (*Camk2a*) gene, were used to generate forebrain-specific knockout mice of *Xrn1* (Casanova et al., 2001). To generate *Xrn1*-cKO mice, we crossed *Xrn1*$^{flox/flox}$ mice with *Camk2a-Cre*$^{+/-}$mice. Primers used for genotyping of wild-type and floxed alleles are listed in Table S2. All mice were maintained under a 12-hr light/12-hr dark cycle in a temperature-controlled (22°C) barrier facility with free access to water and normal rodent chow (NCD, CA1- 1, CLEA Japan). For diet-induced obesity experiments, 8-week-old mice were fed with high-fat diet (HFD32, CLEA Japan) for 12 weeks. For fasting experiment, mice were fasted for 24 hours. Genders and ages of mice used for experiments are indicated in figure legends. Mouse experiments were approved

by the respective Institutional Animal Care and Use Committees of Okinawa Institute of Science and Technology Graduate University (OIST) and RIKEN Kobe branch.

METHOD DETAILS

Daily food intake analysis

Prior to measuring daily food intake, animals were caged individually and kept under a normal 12-hours light-dark cycle. After at least one day of acclimation, the mass of food intake for 24 hours of *Xrn1*$^{flox/flox}$ (n=10), *Camk2a-Cre* (n=10) and *Xrn1*-cKO (n=10) mice was measured. The daily food intake was determined by subtracting the mass of food remaining after 24 hours from that supplied at the beginning.

Histochemistry

Mouse inguinal white adipose tissue (iWAT), epididymal white adipose tissue (eWAT), brown adipose tissue (BAT) and livers from 23-week-old *Xrn1*$^{flox/flox}$ and *Xrn1*-cKO mice were fixed in 4% paraformaldehyde in phosphate buffer for 24 hours and embedded in paraffin. Paraffin sections (3 μm thick) were stained with hematoxylin and eosin (HE), and histological images of mouse tissues were acquired using a Keyence BZ-x710 at magnifications of 20X (iWAT, eWAT and liver) and 40X (BAT). Adipocyte size in iWAT and eWAT was determined by quantifying bright field images using the hybrid cell count software (Keyence) according to the manufacturer's instructions. Paraffin sections for immunohistochemistry were rehydrated and incubated with 3% H_2O_2 for 10 minutes at room temperature. Slides were boiled for 5 minutes with 0.01 M citrate buffer (pH 6.0) and incubated with blocking buffer (PBS containing 10% goat serum, 0.1% Triton X-100, and 5% BSA fraction V) for 30 minutes at room temperature. Slides were then incubated with blocking buffer containing the antibody against UCP1 (#ab10983; Abcam) overnight at 4°C. After washing in PBS, slides were incubated with biotinylated goat anti-rabbit IgG and subsequently with VECTASTAIN ABC HRP Kit (PK-4001; Vector Laboratories) according to the manufacturer's instructions. UCP1 was detected with DAB Peroxidase Substrate Kit (SK-4100; Vector Laboratories) according to the manufacturer's instructions and then counterstained with hematoxylin (GHS316; SIGMA).

Leptin administration

To test leptin sensitivity, 5-week-old mice were intraperitoneally injected with leptin (5 μg/g body weight) every day for 5 days (from 4th to 8th day). Daily body weight and food intake were measured. Daily weight gain was normalized by daily body weight.

Blood analysis

Random blood glucose was measured from tail vein blood using a glucometer (Glutest Neo alpha Sensor, Sanwa Kagaku Kenkyusho). Mice used for serum collection were euthanized with isoflurane, and blood was taken from the inferior vena cava. Whole blood was kept at room temperature until it clotted. Then it was centrifuged at 2,000 g for 10 minutes to separate serum. Concentrations of serum insulin and serum leptin were measured with a Mouse Insulin ELISA kit (10-1247-01, Mercodia) and a Mouse Leptin ELISA kit (ab199082, Abcam).

IPGTT and ITT

To test glucose tolerance, mice were fasted for 16 hours. Mice were intraperitoneally injected with glucose (1 g/kg body weight), and blood glucose levels were measured at 0, 15, 30, 60, 90 and 120 minutes using a glucometer. To test insulin tolerance, fed mice were intraperitoneally injected insulin (1 U/kg body weight). Blood glucose levels were measured at 0, 15, 30, 60, 90 and 120 minutes using a glucometer.

Metabolic analysis

Whole-body energy metabolism measurements were performed using a Comprehensive Laboratory Animal Monitoring System (CLAMS) equipped with an Oxymax Open Circuit Calorimeter System (Columbus Instruments, Columbus, OH, USA). Mouse weights were measured and mice were acclimated for 3 days in a metabolic chamber with food and water under a normal 12-hours light-dark cycle. Oxygen consumption (VO2) and carbon dioxide production (VCO2) were monitored for 24 hours. The VO2 and VCO2 values were used to calculate the respiratory exchange ratio (RER). RER was used to assess energy source utilization and energy expenditure (EE) normalized by body weight. Data were analyzed using the CLAX software from Columbus Instruments and visualized using an Excel.

Locomotor activity in home cage

Locomotor activity monitoring in home cage was performed with a system that automatically analyzes the locomotor activity of mice in their home cage (O'Hara & Co., Ltd). The system contains a home cage with a lid harboring a CCD camera and a white and IR LED unit. Mice were housed individually under a normal 12 hours light-dark cycle with free access to both water and food. After a day acclimation, the distance traveled every minute was measured for 24 hours. Images from each cage were captured at a rate of two frames per second and automatically analyzed using a modified ImageJ software from O'Hara & Co., Ltd. Data (Schneider et al., 2012) were exported and visualized using GraphPad Prism.

Immunoblotting

For protein expression analysis, mice were euthanized with isoflurane and perfused with PBS. Tissue was frozen in liquid nitrogen immediately after excision and kept at -80°C until use. Tissue was homogenized in TNE buffer (20 mM Tris-HCl, pH 7.5, 150 mM NaCl, 2 mM EDTA, 1% NP40, EDTA-free Protease Inhibitor Cocktail (Nacalai Tesque), 1 mM PMSF, 1mM β-Glycerophosphate, 1 mM Na_2VO_3, and 1 mM NaF) by passing the tissue in lysis buffer 10 times through a 24-gauge needle, followed by incubation for 30 minutes on ice. Lysates were clarified by centrifugation at 16,000 g for 10 minutes at 4°C. Protein concentrations in lysates were measured using a Pierce BCA protein assay Kit (Thermo Fisher Scientific) and dissolved in 1xSDS sample buffer (containing 3% SDS, 10% glycerol, and 5% β-mercaptoethanol). Proteins in lysates were then reduced at 95°C for 5 minutes before being separated by SDS-polyacrylamide gel (SDS-PAGE) electrophoresis. Proteins transferred onto 0.45μm polyvinylidene difluoride membranes (PVDF, Millipore cat no. IPVH00010) using a wet transfer system (Nihon Eido, Tokyo, Japan). After membranes were blocked with 3% skimmed milk in TBST (20 mM Tris–HCl, pH 7.5, 150 mM NaCl, 0.05% v/v Tween 20), proteins of interest were probed with specific primary antibodies and then appropriate horseradish peroxidase (HRP)-conjugated secondary antibodies. Chemiluminescent signals were detected using an ImageQuant LAS 4000 mini (GE Healthcare, Tokyo). Sequential probing of membranes with a variety of antibodies was performed after inactivation of HRP with 0.1% sodium azide (NaN_3), according to the antibody manufacturer's protocol. Protein level was quantified using ImageJ software and normalized to α-tubulin. The following primary antibodies were used for immunoblotting: XRN1 (A300-443A; Bethyl Laboratories), LEPR (ab177469; Abcam), INSR (#3025; Cell Signaling), STAT3 (#4904; Cell Signaling), SOCS3 (#2923; Cell Signaling), FOXO1 (#2880; Cell Signaling), PTP1B (#5311; Cell Signaling), TCPTP (#58935; Cell Signaling), α-tubulin (#T9026; SIGMA), GAPDH (#2118; Cell Signaling), CNOT1 (#1012; Bio Matrix), CNOT2 (#34214; Cell Signaling), CNOT3 (#54; Bio Matrix), and CNOT7 (H00029883-M01; Abnova). The following secondary antibodies were used: ECL anti-mouse IgG HRP-conjugated whole antibody (NA931V; GE healthcare) and ECL anti-rabbit IgG HRP-conjugated whole antibody (NA934V; GE healthcare).

Quantitative PCR

Quantitative PCR (qPCR) was performed according to the protocol of Taylor et al. (Taylor et al., 2019). 1μg of total RNA was used for cDNA synthesis with SuperScript Reverse Transcriptase III (Thermo Fisher Scientific). cDNA was diluted 10-fold with RNase-free water. qPCR reactions consisted of 2.5 μL of cDNA, 5 μL of SYBR Premix Ex Taq (Takara), 0.2 μL of ROX reference dye, 0.2 μL of 10 μM primers (primers are listed in Tables S3 and S4). qPCR was performed using a ViiA 7 Real-Time PCR System (Applied Biosystems). Target cDNA expression was normalized to both *Gapdh* and *Hprt* using the method of Taylor et al. (2019). Pre-mRNA expression was normalized to both *Gapdh* and *Rplp0*. Each sample was run in three technical replicates.

Immunofluorescence

Mice were euthanized with isoflurane and perfused with 4% PFA/PBS. After perfusion, brains were dissected and further fixed in 4% PFA/PBS overnight at 4°C. Fixed brains were immersed in 15% sucrose/PBS for 2 hours at 4°C and 30% sucrose/PBS overnight at 4°C. Brains were embedded in optimal cutting temperature (OCT) compound and frozen at -20°C. Frozen brains were sectioned coronally at 30 μm using a Leica CM 3050S cryostat. Brain sections were kept in PBS at 4°C until use. Brain sections were mounted on slides, and then washed twice with PBS. After blocking in PBS with 0.05% Triton X-100 (PBS-T) containing 5% goat serum for 1 hour at RT, sections were incubated with antibodies against XRN1 (A300-443A; Bethyl Laboratories), or AgRP (H-003-57; Phoenix Pharmaceuticals) at 4°C overnight. After washing in PBS-T, slides were incubated with secondary antibody (Goat Anti-Rabbit IgG H&L (Alexa Fluor® 555); ab150078; Abcam) for 2 hours at RT. Slides were then washed in PBS-T and incubated with

DAPI. Immunolabelling was detected by fluorescence microscopy using a Keyence BZ-X700. Signal intensities were quantified from images using ImageJ software.

QUANTIFICATION AND STATISTICAL ANALYSIS

Statistical analyses were conducted using an unpaired two-tailed Student's t test, one-way ANOVA followed by Tukey post hoc test or two-way ANOVA followed by Bonferroni post hoc test as indicated in the figure legends. All values < 0.05 were considered significant.